

Reversible Perovskite Electrocatalysts for Oxygen Reduction / Oxygen Evolution

Kieren Bradley¹, Kyriakos Giagloglou¹, Brian E Hayden^{1,2*}, Hugo Jungius¹, Chris Vian¹

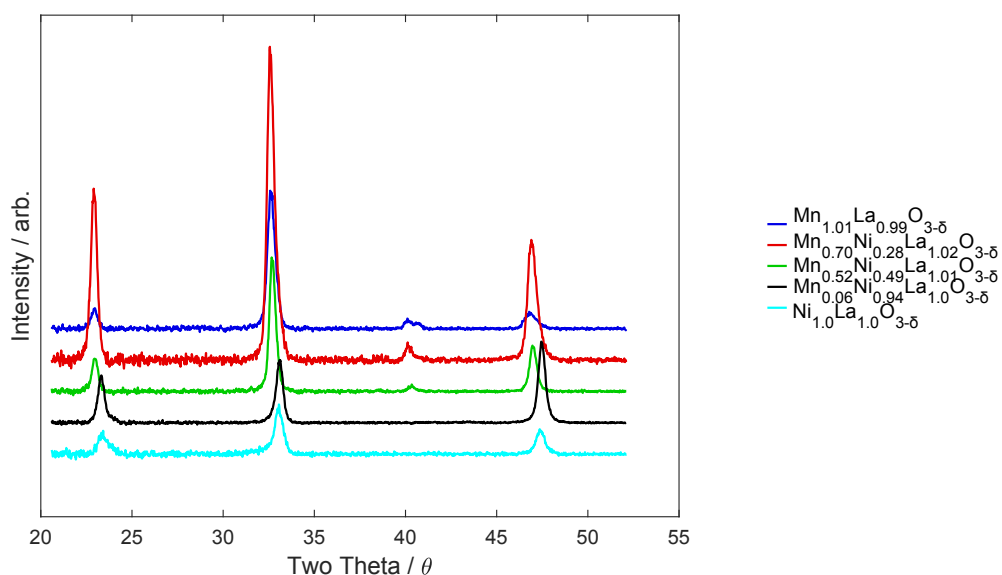
¹ Ilika Technologies, Kenneth Dibben House, Enterprise Road, Southampton Science Park, Southampton. SO16 7NS, UK.

² Chemistry, University of Southampton, Highfield, Southampton, SO17 1BJ, UK.

SUPPLEMENTARY INFORMATION

Structural Characterisation of $\text{La}_x\text{Mn}_y\text{Ni}_{1-y}\text{O}_{3-\delta}$ Perovskites

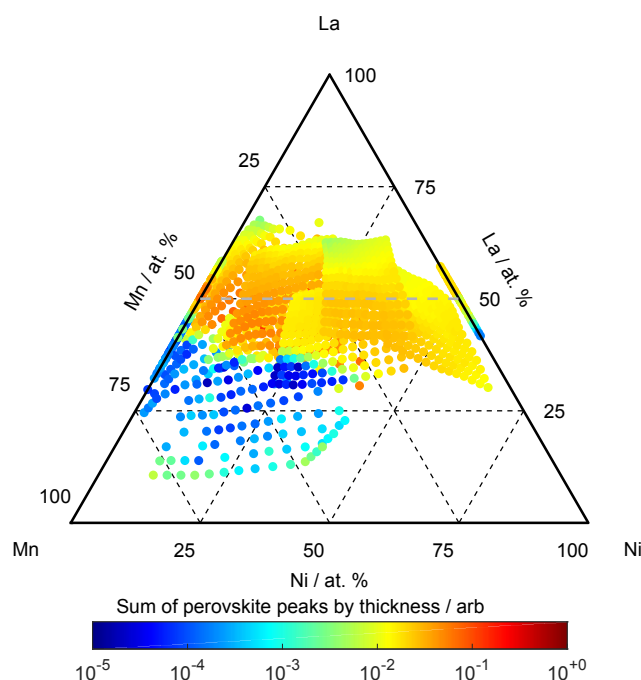
X-ray diffraction patterns were recorded (2θ values between 21° and 52°) on both Si/SiO and electrochemical substrates: The structure for similar compositions was found to be the same irrespective of the substrate. XRD patterns were collected with 2θ values between 21° and 52° , within this range only 6 clearly defined peaks were found. A series of XRD measurements taken along the pseudo-binary line indicate that the perovskite is synthesised exclusively at all compositions and characterised by the four Bragg peaks (100), (110), (111) and (200). We do not observe any of the other phases observed elsewhere.²¹ Bragg peaks associated with NiO and MnO_2 phases are only observed at compositions with less than 30 a.t.% La, well



away from the pseudo-binary line.

Supplementary Information I XRD patterns along the pseudo-binary line of $\text{La}_x\text{Mn}_y\text{Ni}_{1-y}\text{O}_{3-\delta}$ indicate that the perovskite is synthesised exclusively at all compositions and characterised by the four Bragg peaks (100), (110), (111) and (200). Data has been obtained from XRD of $\text{La}_x\text{Mn}_y\text{Ni}_{1-y}\text{O}_{3-\delta}$ catalysts synthesised on Si/SiO substrates.

A logarithmic plot of the sum of the three major perovskite peak intensities (110), (111) and (200) peaks at $2\theta = 32.5^\circ$, 40° and 47° respectively, and shows the compositional regions dominated by the perovskite structure: The sum of the three peaks are chosen in order to overcome the substrate induced orientation effects observed with compositional change, and which influence the relative peak intensities. It is evident that the $\text{La}_x\text{Mn}_y\text{Ni}_{1-y}\text{O}_{3-\delta}$ perovskites can accommodate a wide range of Mn / La sub-stoichiometry.



Supplementary Information II Ternary plot of the sum of the three major perovskite 2θ peaks (32.5° , 40° , and 47°) with a logarithmic scale that shows the presence of perovskite structure of $\text{La}_x\text{Mn}_y\text{Ni}_{1-y}\text{O}_{3-\delta}$. The data has been obtained from XRD on 12 individual compositional gradient thin film libraries of $\text{La}_x\text{Mn}_y\text{Ni}_{1-y}\text{O}_{3-\delta}$ synthesised at 550°C on Si/SiO substrates.

A plot of the 2θ position of the (110) Bragg peak of the perovskite as a function of composition in a ternary plot, and as a function of Ni substitution along the pseudo-binary line of $\text{La}_x\text{Mn}_y\text{Ni}_{1-y}\text{O}_{3-\delta}$. Along the pseudo-binary composition line there is a linear dependence of the (110) 2θ position which correspond to a gradual change from the cubic LaMnO_3 (Pm-3m) to the rhombohedral LaNiO_3 (R-3c) lattice: The solid line represents a linear dependence between the two structures.⁴¹⁻⁴² For compositions below ca. 10% Ni, however, there is a large scatter in the data towards higher 2θ values. There is also a range of 2θ values obtained for the cubic LaMnO_3 (Pm-3m) which corresponds to a smaller lattice dimension that would be expected.⁴² We suggest that this is a result of La^{3+} substitution by Mn^{2+} at the A-site. Note that this predominates at even slightly La poor compositions in LaMnO_3 . It is interesting to note (Figure 2A) that in the ternary compositions, there is also a region of La sub-stoichiometric compositions in the Ni poor composition region (up to $y = 0.2$ in $\text{La}_x\text{Mn}_y\text{Ni}_{1-y}\text{O}_{3-\delta}$) where the

(110) 2θ angle remains constant near to the value for LaMnO₃. A likely explanation for this is that either Ni²⁺ or Mn²⁺ ions are also being co-ordinated in the La A-site, leading to a compensation in the lattice size as the B-site is accommodating Ni³⁺. Moreover, Mn²⁺ and Ni²⁺

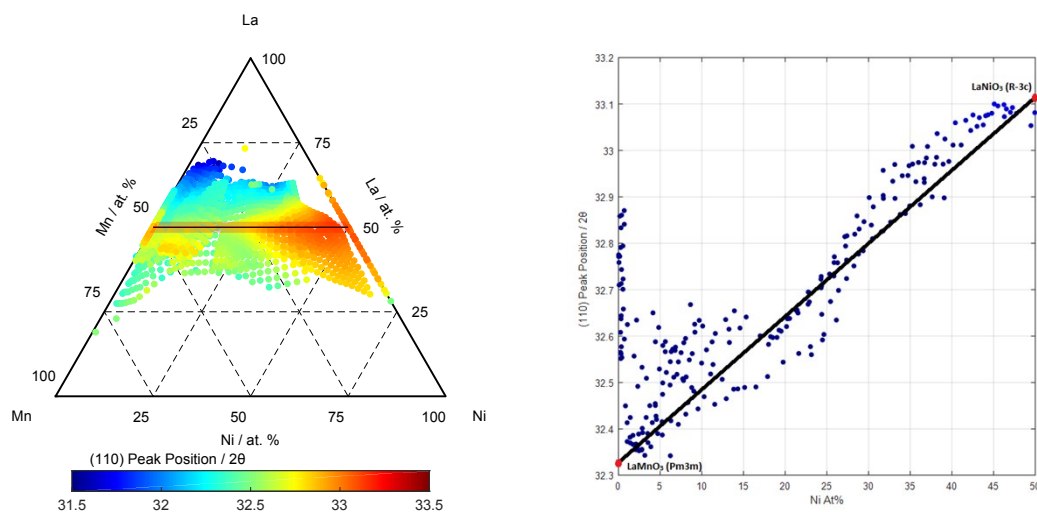
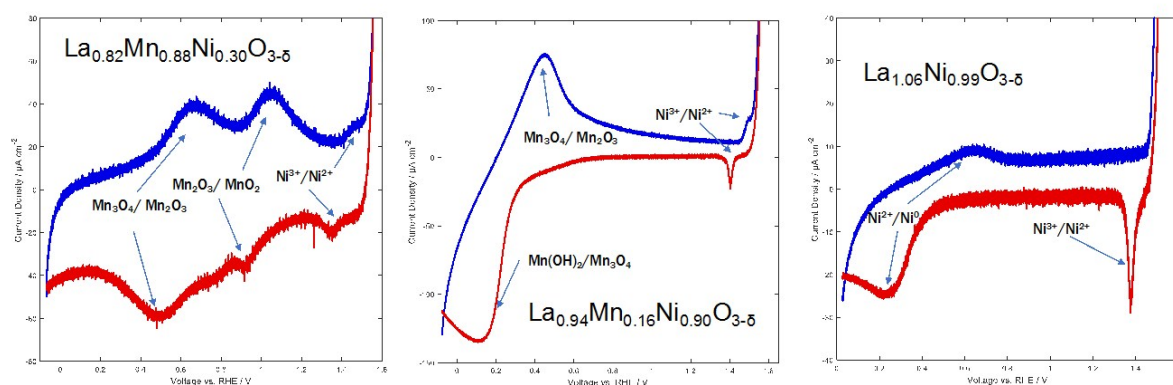


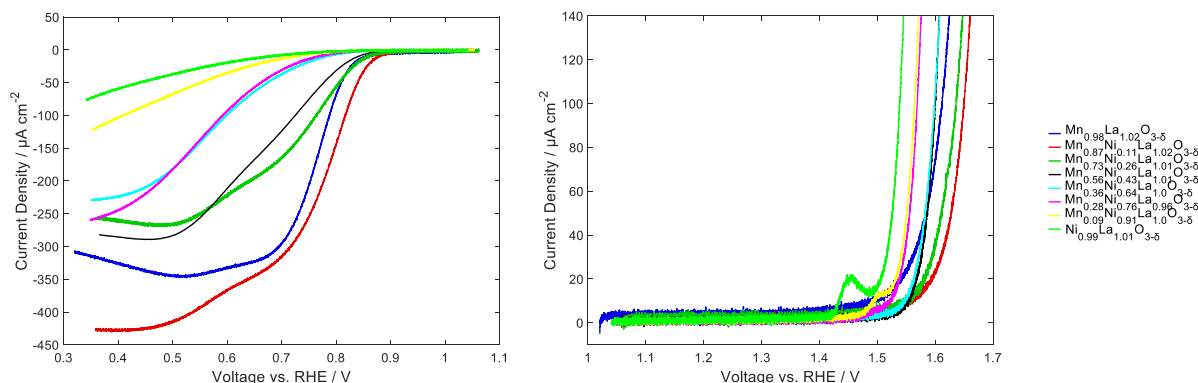
exhibit same ionic radius (70 pm)³⁴ and could be either Mn²⁺ or Ni²⁺ on the A-site. Mn²⁺ has been substituted on the A-site in the LaMnO₃,⁴⁴⁻⁴⁵ in the Ca_{1-x}Mn_xTiO₃⁴⁶ and in the Sr_{1-x}Mn_xTiO₃ system.⁴⁷

Supplementary Information III A) The compositional dependence of the (110) 2θ peak position of the perovskite as a function of composition for La_xMn_yNi_{1-y}O_{3-δ}. B) The compositional dependence of the (110) 2θ peak position of the perovskite along the pseudo-binary tie-line (±2 at%) of La_xMn_yNi_{1-y}O_{3-δ}. The black line indicates the limits of (110) 2θ peak position between LaMnO₃ (Pm-3m)³³ and LaNiO₃ (R-3c) [H. Falcon et al., Journal of Solid State Chemistry (1997) 133, 379-385]. The data has been obtained from XRD on 12 individual compositional gradient thin film libraries of La_xMn_yNi_{1-y}O_{3-δ} synthesised at 550 °C on Si/SiO₂ substrates.

Cyclic Voltammetry of La_xMn_yNi_{1-y}O_{3-δ} Perovskites



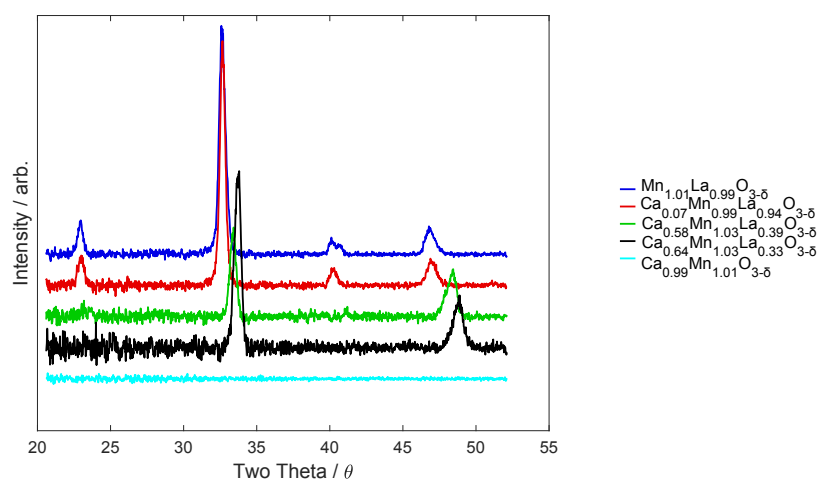
Supplementary Information IV Selected cyclic voltammograms (5 mVs⁻¹ scan rate, room temperature) recorded in deoxygenated 0.1 M KOH at various compositions of the La_xMn_yNi_{1-y}O_{3-δ} thin film electrocatalysts showing the most prominent redox couples in the system.



Supplementary Information V. A) The currents associated with: A) The Oxygen Reduction Reaction (ORR) measured in the cathodic scan and B) The Oxygen Evolution Reaction (OER) measured for a selection of the compositions of the $\text{La}_x\text{Mn}_y\text{Ni}_{1-y}\text{O}_{3-\delta}$ thin film electrocatalyst. Measurements have been made at a scan speed of 5 mVs^{-1} in oxygen saturated 0.1M KOH at 25°C .

Structural Characterisation of $\text{La}_x\text{Ca}_{1-x}\text{Mn}_y\text{O}_{3-\delta}$ Perovskites

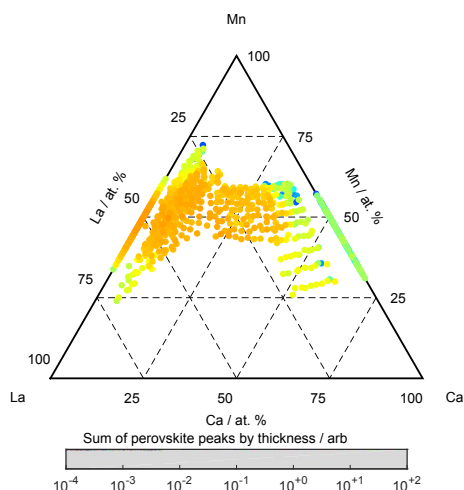
A series of the $\text{La}_x\text{Ca}_{1-x}\text{Mn}_y\text{O}_{3-\delta}$ perovskite libraries were synthesised, and characterised by X-ray diffraction on both Si/SiO_2 and electrochemical substrates for the $\text{La}_x\text{Ca}_{1-x}\text{Mn}_y\text{O}_{3-\delta}$. The XRD patterns were collected with 2θ values between 21° and 52° : within this range only 4 clearly defined peaks were found at 23° , 32.5° , 40° and 47° corresponding to the orthorhombic perovskite (Pnma)⁵³ Bragg peaks (100), (110), (111) and (200).



Supplementary Information VI. XRD patterns along the pseudo-binary line of $\text{La}_x\text{Ca}_{1-x}\text{Mn}_y\text{O}_{3-\delta}$ indicate that the perovskite is synthesised exclusively at all compositions and characterised by the four Bragg

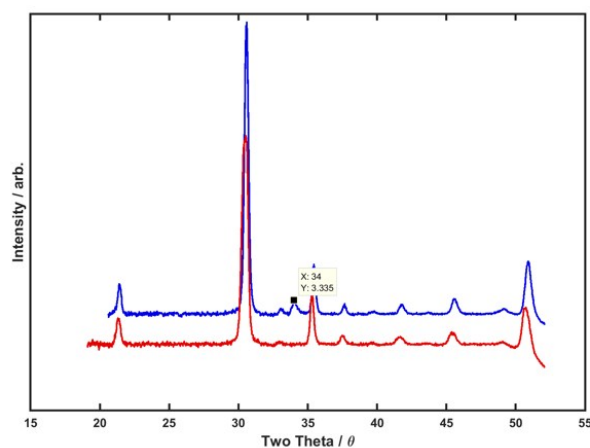
peaks (100), (110), (111) and (200). Data has been obtained from XRD of $\text{La}_x\text{Ca}_{1-x}\text{Mn}_y\text{O}_{3-\delta}$ catalysts synthesised on $\text{Si}\backslash\text{SiO}$ substrates.

The compositional region where perovskites were observed are shown through a logarithmic plot of the sum of the (110), (111) and (200) peak areas to account any texturing of the thin films as for the case of the $\text{La}_x\text{Mn}_y\text{Ni}_{1-y}\text{O}_{3-\delta}$ catalysts (above). A sharp cut off in the presence of the perovskite is seen at higher calcium content with no perovskite peaks observed for compositions where the Ca:La ratio was greater than ca. 3:1.



Supplementary Information VII Ternary plot of the sum of the three major perovskite 2 θ peaks (32.5°, 40°, and 47°) with a logarithmic scale that shows the presence of perovskite structure of $\text{La}_x\text{Ca}_{1-x}\text{Mn}_y\text{O}_{3-\delta}$. The data has been obtained from XRD on 9 individual compositional gradient thin film libraries of $\text{La}_x\text{Ca}_{1-x}\text{Mn}_y\text{O}_{3-\delta}$ synthesised at 550 °C on the ITO of the electrochemical array substrate.

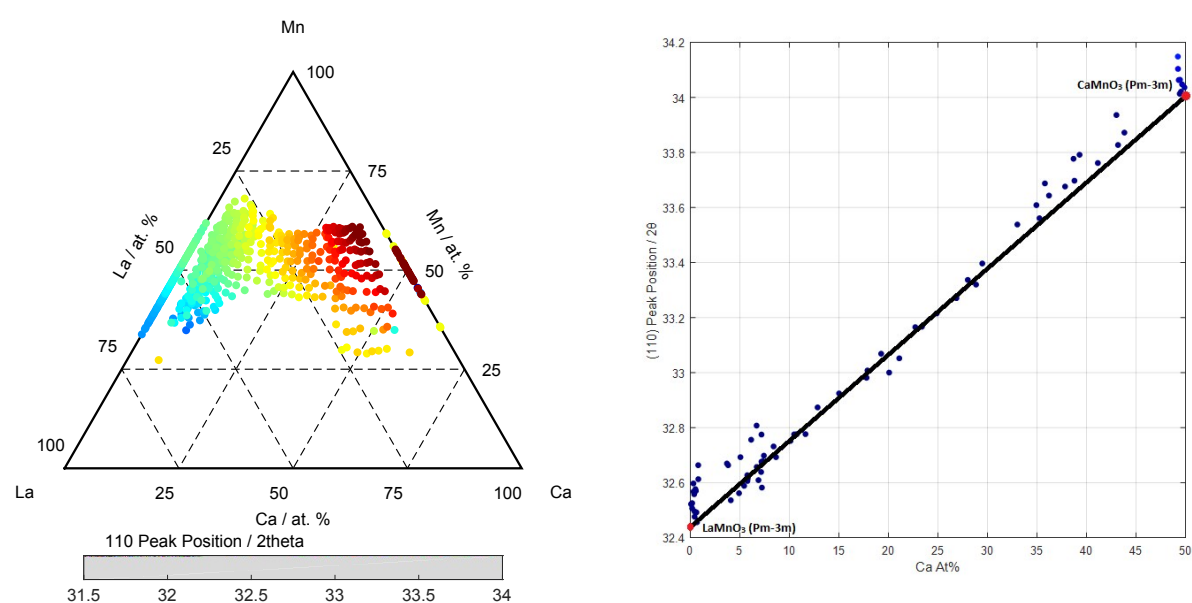
The diffraction patterns pertaining to compositions Ca:La > 3:1 do not show the presence of peaks at any measured range, but are likely to be poorly crystallised perovskites: A library in this composition region was annealed, post deposition, at 800 °C in the presence of oxygen to promote crystallisation resulting in the appearance of a weak XRD peak corresponding to the (110) perovskite Bragg peak. There was a minimal change observed in the



electrochemical performance following post annealing.

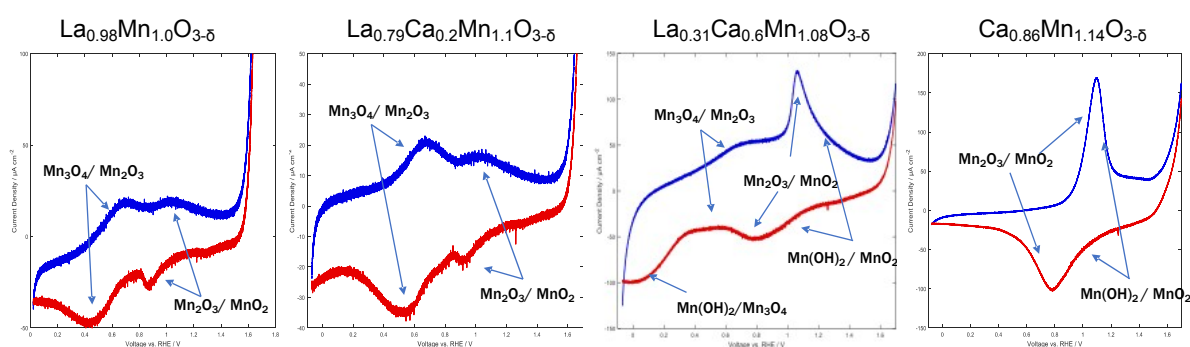
Supplementary Information VIII XRD patterns for $\text{La}_{0.1}\text{Ca}_{0.68}\text{Mn}_{1.36}\text{O}_{3-\delta}$ A) As synthesised and B) following a post anneal at 800 °C. The $\text{La}_{0.1}\text{Ca}_{0.68}\text{Mn}_{1.36}\text{O}_{3-\delta}$ has been synthesised on the ITO substrate of the electrochemical array. At these Ca rich compositions, the perovskite is not crystallised before annealing, and starts to crystallise after post annealing. The marked peak corresponds to the (110) Bragg peak of the cubic structure.

Along the perovskite pseudo-binary composition line $\text{La}_x\text{Ca}_{1-x}\text{Mn}_y\text{O}_{3-\delta}$, a continuous A-site substitution in a cubic (Pm-3m) to orthorhombic (Pnma) perovskite solid solution is exhibited: this is directly evidenced in the linear shift in the (110) Bragg peak position peak as a function of composition.

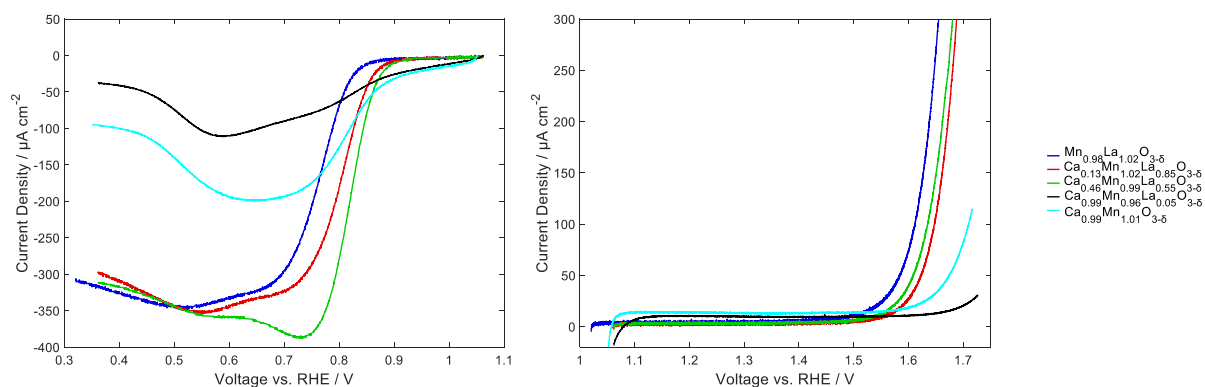


Supplementary Information IX. A) The compositional dependence of the (110) 2θ peak position of the perovskite as a function of composition for $\text{La}_x\text{Ca}_{1-x}\text{Mn}_y\text{O}_{3-\delta}$. B) The compositional dependence of the (110) 2θ peak position of the perovskite along the pseudo-binary tie-line (± 2 at%) of $\text{La}_x\text{Ca}_{1-x}\text{Mn}_y\text{O}_{3-\delta}$. The black line indicates the limits of (110) 2θ peak position between LaMnO_3 (Pm-3m) ³³ and CaMnO_3 (Pm-3m) [Mishra et al. Physical Review B (2016) 93, 214306]. The data has been obtained from XRD on 9 individual compositional gradient thin film libraries of $\text{La}_x\text{Ca}_{1-x}\text{Mn}_y\text{O}_{3-\delta}$ synthesised at 550 °C on the ITO of the electrochemical array substrate.

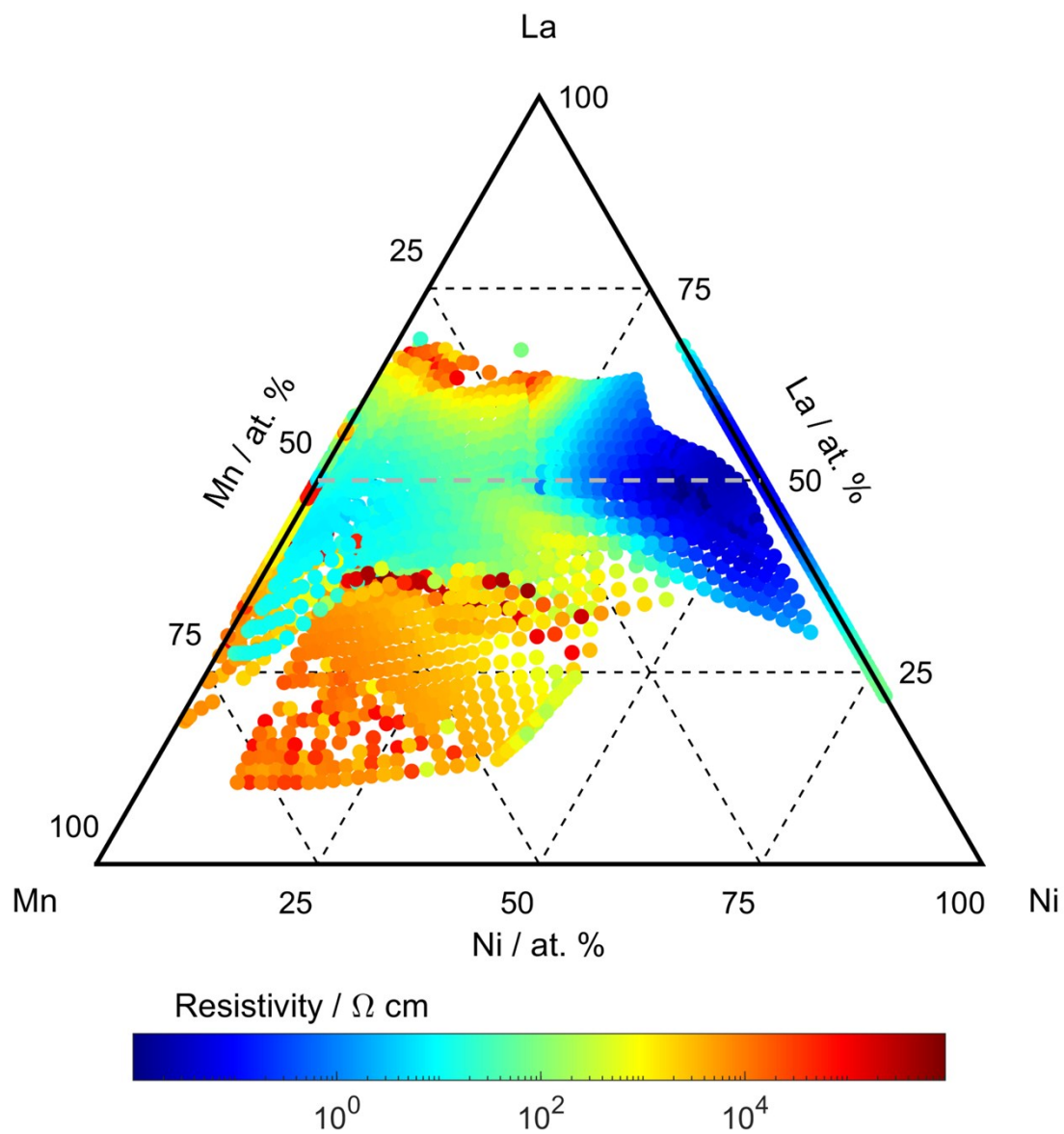
Cyclic Voltammetry of $\text{La}_x\text{Ca}_{1-x}\text{Mn}_y\text{O}_{3-\delta}$ Perovskites



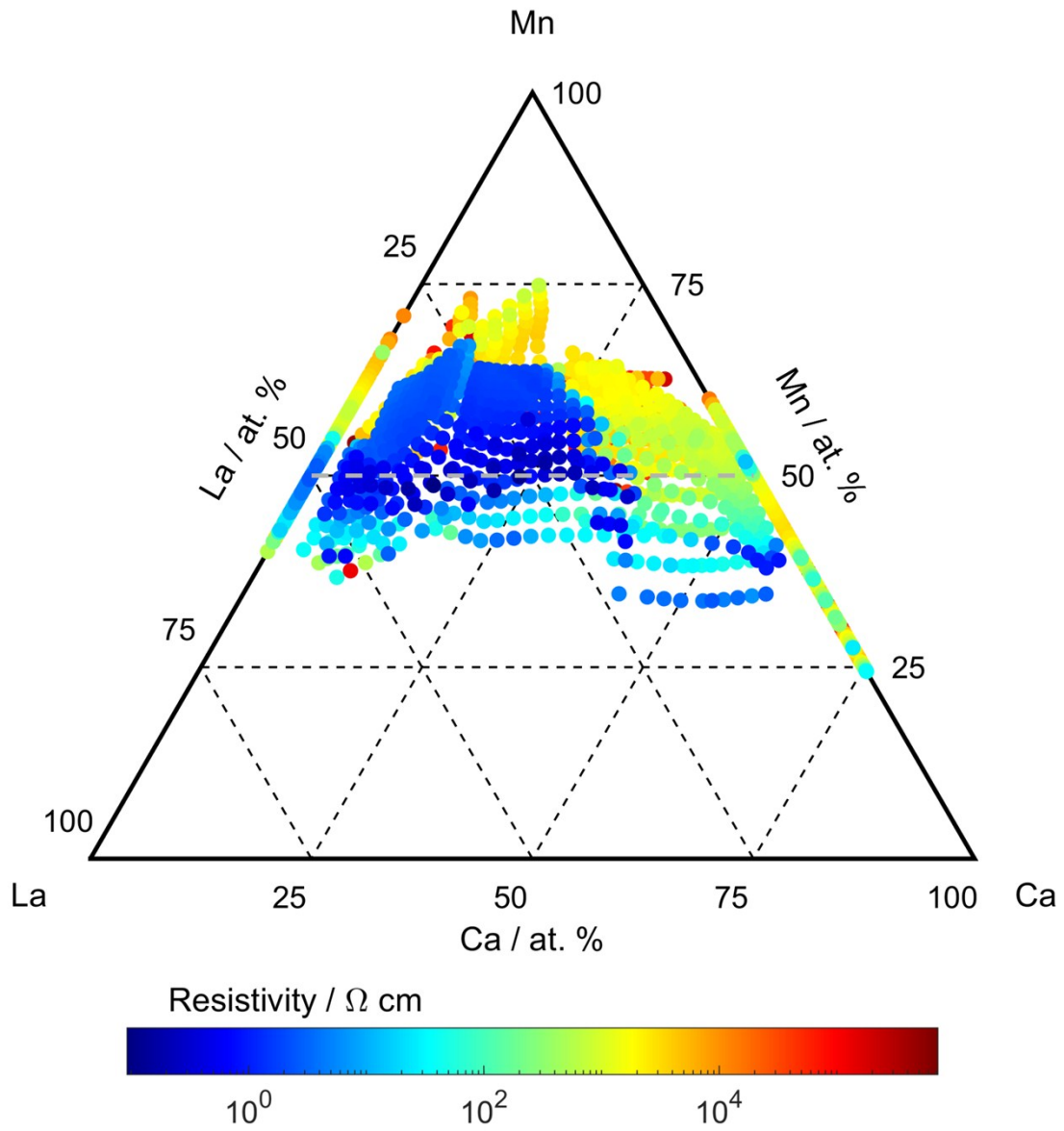
Supplementary Information X Selected cyclic voltammograms (5 mVs^{-1} scan rate, room temperature) recorded in deoxygenated 0.1 M KOH at various compositions of the $\text{La}_x\text{Ca}_{1-x}\text{Mn}_y\text{O}_{3-\delta}$ thin film electrocatalysts showing the most prominent redox couples in the system.



Supplementary Information XI. A) The currents associated with: A) The Oxygen Reduction Reaction (ORR) measured in the cathodic scan and B) The Oxygen Evolution Reaction (OER) measured for a selection of the compositions of the $\text{La}_x\text{Ca}_{1-x}\text{Mn}_y\text{O}_{3-\delta}$ thin film electrocatalyst. Measurements have been made at a scan speed of 5 mVs^{-1} in oxygen saturated 0.1 M KOH at 25°C .



Supplementary Information XII. Compositional dependence of the resistivity of the $\text{La}_x\text{Mn}_y\text{Ni}_{1-y}\text{O}_{3-\delta}$ thin films. Measured using a linear four-point probe on libraries deposited on silicon / silicon oxide substrates.



Supplementary Information XIII. Compositional dependence of the resistivity of the $\text{La}_x\text{Ca}_{1-x}\text{Mn}_y\text{O}_{3-\delta}$ thin films. Measured using a linear four-point probe on libraries deposited on silicon / silicon oxide substrates.